J. Ocean Univ. China (Oceanic and Coastal Sea Research)
https://doi.org/10.1007/s11802-019-3829-2
ISSN 1672-5182, 2019 18 (2): 365-375
http://www.ouc.edu.cn/xbywb/
E-mail:xbywb@ouc.edu.cn

Evaluation of Typhoon Waves Simulated by WaveWatch-III Model in Shallow Waters Around Zhoushan Islands

SHENG Yexin[1), 2)], SHAO Weizeng[1), *], LI Shuiqing[2), 3)], ZHANG Yuming[4)], YANG Hongwei[5)], and ZUO Juncheng[1)]

1) *Marine Science and Technology College*, *Zhejiang Ocean University*, *Zhoushan* 316000, *China*
2) *Institute of Oceanology*, *Chinese Academy of Sciences*, *Qingdao* 266071, *China*
3) *Laboratory for Ocean Dynamics and Climate*, *Qingdao National Laboratory for Marine Science and Technology*, *Qingdao* 266071, *China*
4) *National Marine Environmental Monitoring Center*, *State Oceanic Administration*, *Dalian* 116023, *China*
5) *Shandong University of Science and Technology*, *Qingdao* 266590, *China*

(Received February 12, 2018; revised May 24, 2018; accepted May 31, 2018)

Abstract In this study, we simulated typhoon waves in the shallow waters around the Zhoushan Islands using the WaveWatch-III (WW3) model version 5.16, the latest version released by the National Oceanic and Atmospheric Administration. Specifically, we used *in-situ* measurements to evaluate the performance of seven packages of input/dissipation source terms in the WW3 model. We forced the WW3 model by wind fields derived from a combination of the parametric Holland model and high-resolution European Center for Medium-Range Weather Forecasts (ECMWF) wind data in a 0.125° grid, herein called H-E winds. We trained the H-E winds by fitting a shape parameter B to buoy-measured observations, which resulted in a smallest root mean square error (*RMSE*) of 3 m s^{-1} for B, when treated as a constant 0.4. Then, we applied the seven input/dissipation terms of WW3, labelled ST1, ST2, ST2+STAB2, ST3, ST3+STAB3, ST4, and ST6, to simulate the significant wave height (SWH) up to 5 m during typhoons Fung-wong and Chan-hom around the Zhoushan Islands. We then compared the SWHs of the simulated waves with those measured by the *in-situ* buoys. The results indicate that the simulation using ST2 performs best with an *RMSE* of 0.79 m for typhoon Fung-wong and an *RMSE* of 1.12 m for typhoon Chan-hom. Interestingly, we found the simulated SWH results to be relatively higher than those of the observations in the area between Hangzhou Bay and the Zhoushan Islands. This behavior is worthy of further investigation in the future.

Key words waves; typhoon; WaveWatch-III; Zhoushan Islands

1 Introduction

Typhoons play an important role in water mass and heat transport at the atmospheric-marine boundary layer. However, typhoon waves pose an immediate threat to nearshore regions. The WaveWatch model is a third-generation numeric wave model developed in the spirit of the previous WAM model (The WAMDI Group, 1988) by solving the wave propagation balance equation (Tolman and Booij, 1998; Guan, 2000). The WaveWatch-I model was developed by Hendrik Tolman at Delft University and the updated WaveWatch-II model was released by Goddard Space Flight Center of the National Aeronautics and Space Administration in the early 1990s. The third-generation WaveWatch-III (WW3) model was developed by the National Oceanic and Atmospheric Administration/ National Centers for Environmental Prediction (NOAA/ NCEP) and a similar wave model, called Simulating Waves Nearshore (SWAN), was developed by the Delft University of Technology. The SWAN model is widely used for simulating nearshore waves, whereas the WW3 model performs well in offshore open seas, *e.g.*, Pacific Ocean waves (Bi *et al*., 2015). Analyses of wave characteristics in the South China Sea using the WW3 model have shown that the simulations are consistent with TOPEX/ Poseidon altimeter measurements and *in-situ* buoys (Qi *et al*., 2003; Zhou *et al*., 2014). Recently, the WW3 model has been shown to be capable of simulating the characteristics of typhoon waves (Xu *et al*., 2005; Kong *et al*., 2013; Zhou *et al*., 2014; Liu *et al*., 2017). The new version of the WW3 model, 5.16, was released on October 2016 and differs from its predecessor in several respects, *e.g.*, governing equations, model structure, numerical methods, and physical parameterization (The WAVEWATCH-III Development Group, 2016). In particular, its devel-

* Corresponding author. E-mail: shaoweizeng@zjou.edu.cn

opments include stress-calculations dependence on various sea states, a new nonlinear wave-wave interaction source term called two-scale approximation, and the capability for calculating space-time extremes. These improvements have a definite impact on wave simulations, especially in typhoons.

In this study, we simulated waves using the latest released version WW3 model in typhoons Fung-wong in 2014 and Chan-hom in 2015. Both these typhoons crossed the East China Sea, and typhoon Chan-hom, in particular, landed at the Zhoushan Islands, around which the water depth is less than 100 m. To obtain reasonable wind fields in typhoons, we used the parametric Holland model (Holland, 1980) and the European Center for Medium- Range Weather Forecasts (ECMWF) wind data in a 0.125° grid, herein referred to as H-E winds. To validate the simulated winds and waves, we used measurements from five *in-situ* buoys around the Zhoushan Islands taken during the periods of the two typhoons.

The remainder of this paper is organized as follows: we briefly describe the available dataset in Section 2. We present our methodology for deriving the H-E wind fields in Section 3. In Section 4, we present the wave simulations and validations using the seven source terms of the WW3 model, and we conclude by summarizing our findings in Section 5.

2 Description of Dataset

In our work, we simulated waves in the East China Sea during the periods of typhoons Fung-wong in 2014 and Chan-hom in 2015. The simulated area is located between (21°N, 117°E) and (34°N, 131°E) and the bathymetric topography of this area is provided by the General Bathymetry Chart of the Oceans (GEBCO) with a high-spatial-resolution 0.01° grid, as shown in Fig.1.

Since 1979, the ECMWF has provided continuous daily reanalysis wind data with a 0.125°×0.125° spatial resolution at 6-h intervals. In our previous study, we used ECMWF wind data at 10 m above the sea surface to simulate waves and enable an analysis of the global wind-sea and swell energy distribution using the WW3 model (Zheng *et al*., 2016). The best track data of typhoons Fung-wong and Chan-hom were collected by the Regional Specialized Meteorological Center (RSMC) Tokyo-Typhoon Center of Japan Meteorological Agency (JMA), which provides the locations of typhoon centers, central pressures, and maximum wind radii. Fig.2 shows the tracks of typhoons Fung-wong and Chan-hom, both of which crossed the Zhoushan Islands. In this study, we found the maximum wind speeds from ECMWF to be less than those from the JMA best track data. Therefore, we used the parameters from the JMA best track data to build wind fields with the parametric Holland model and ECMWF grid. To force the WW3 model in our study, we chose large values between the ECMWF winds data and simulated Holland winds to obtain H-E wind fields. As an example, Figs.3a and 3b show the H-E wind fields of typhoon Fung-wong on September 22, 2014 at 12:00 UTC and of typhoon Chan-hom on July 11, 2015 at 06:00 UTC.

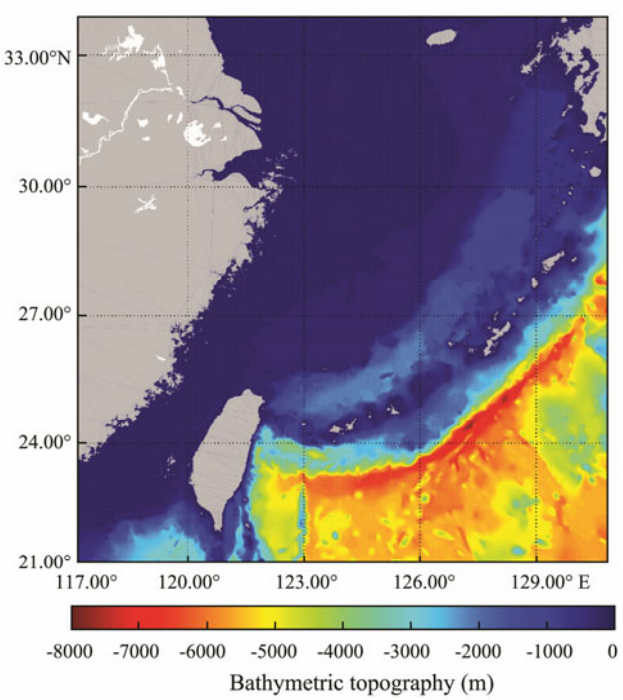

Fig.1 Bathymetric topography of the East China Sea with high spatial resolution in a 0.01° grid in the area between 21°–34°N, 117°–131°E, as provided by GEBCO. The color indicates the bathymetric topography.

We collocated the wind and wave data from *in-situ* buoys around the Zhoushan Islands during the periods of the two typhoons, which we used to validate the H-E winds and waves simulated by the WW3 model with different source terms. The locations of the *in-situ* buoys, labeled B10 to B14, are shown in Fig.4, where we can see that the water depth is less than 100 m around the Zhoushan Islands.

3 Derivation of H-E Winds

To obtain reasonable H-E winds, we performed a combinned analysis of the simulation results from the parametric Holland model and ECMWF winds. We trained the H-E winds with four different shape parameters and validated the results against data from the five collocated in-situ buoys during typhoons Fung-wong and Chan-hom.

3.1 Holland Model

Holland (1980) proposed an analytical model for obtaining wind and pressure profiles in cyclones. This model is mainly based on the maximum wind radius and pressure difference, and it contains two empirical scaling parameters A and B. The model is expressed as follows:

$$V_g = \left[\frac{AB\left(p_n - p_c\right)e^{-A/r^B}}{\rho r^2} + \frac{r^2 f^2}{4} \right]^{1/2} - \frac{rf}{2}, \qquad (1)$$

where V_g is the sea surface wind speed at radius r; p_c is

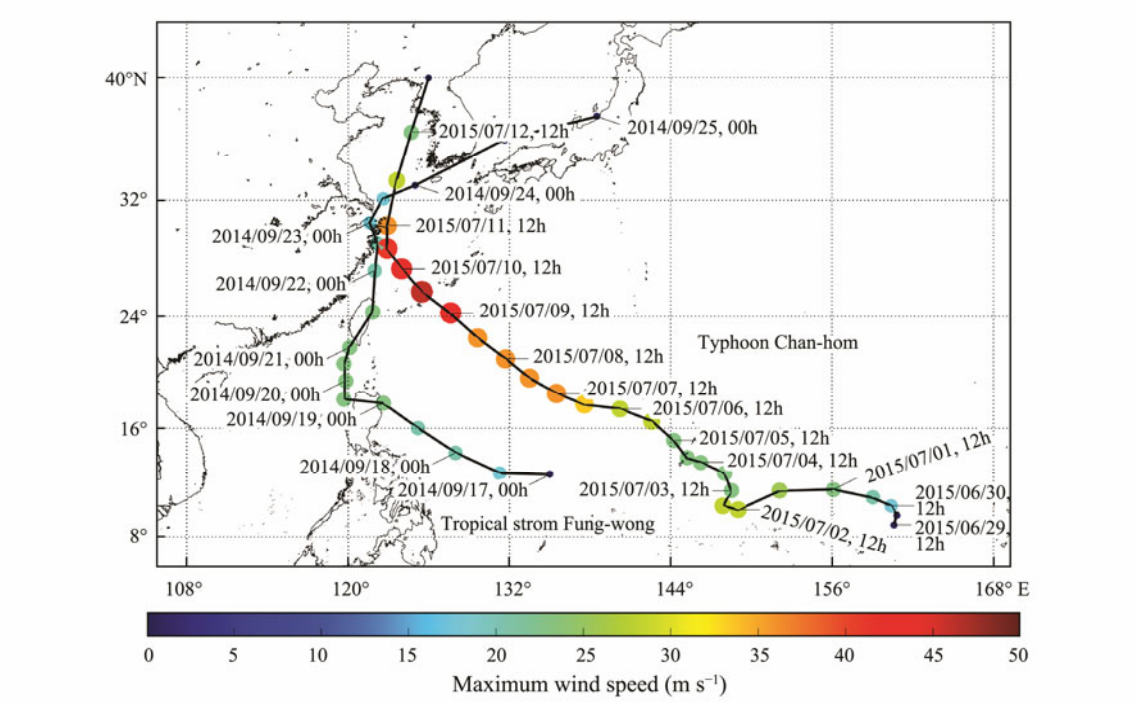

Fig.2 Tracks of tropical cyclone Fung-wong and typhoon Chan-hom crossing the East China Sea. The colors and sizes of the circles indicate the maximum wind speed of typhoons Chan-hom and Fung-wong.

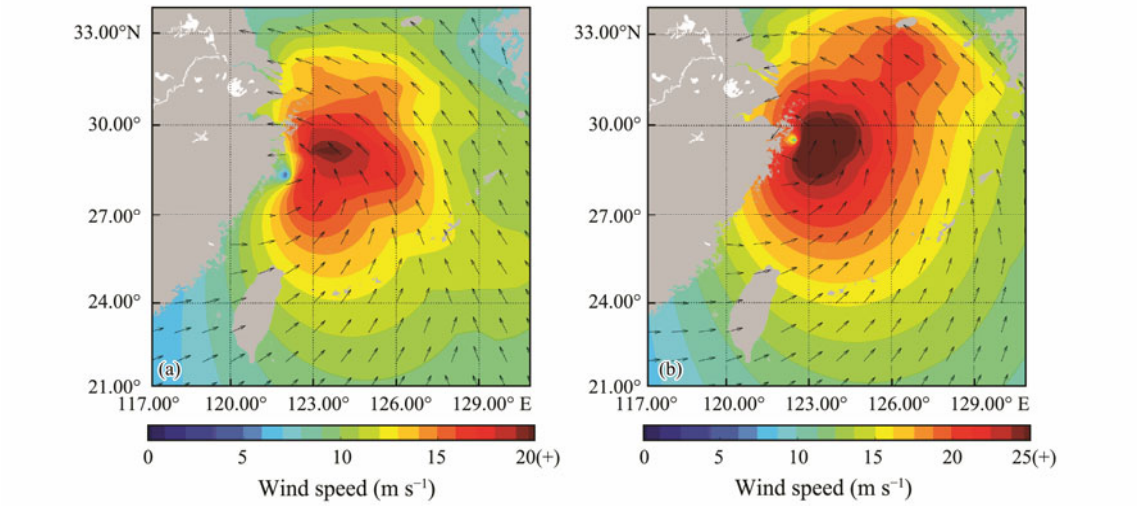

Fig.3 H-E wind fields of typhoon Fung-wong on September 22, 2014 at 12:00 UTC (a) and typhoon Chan-hom on July 11, 2015 at 06:00 UTC (b). The colors indicate the wind speeds.

the central pressure of typhoon; p_n is the ambient pressure, which is theoretically the pressure at infinity (=1015 hPa); f is the Coriolis force parameter at latitude, and ρ is the air density constant (=1.15 kg m^{-3}). In addition, Holland (1980) proposed that the maximum wind radius can be defined by the empirical scaling parameters A and B, as follows:

$$A = r_{\max}^{B} \quad , \tag{2}$$

where A determines the location relative to the origin, B determines the shape of the cyclone, and $r_{\max}$ represents the maximum wind radius. To satisfy various sea states, it is necessary to determine if the empirical scaling parameter B can be trained over a range from 0.4 to 1 at intervals of 0.2.

By taking Eq. (2) into Eq. (1), we can calculate wind speed by the location of the cyclone center, the central pressure of the cyclone p_c, the maximum wind speed, and the scaling parameter B. Wind direction is calculated by the 15° spiral directions of the cyclone (Zec and Jones, 2000). Next, the wind vectors simulated using the Holland model must be synthesized with the speed of the cyclone center movement, as follows:

$$\vec{V} = \vec{V_m} + \vec{V_g} \ , \tag{3}$$

where V_m is the cyclone movement speed. The composite

wind vectors are the final wind fields in the typhoons used in our study.

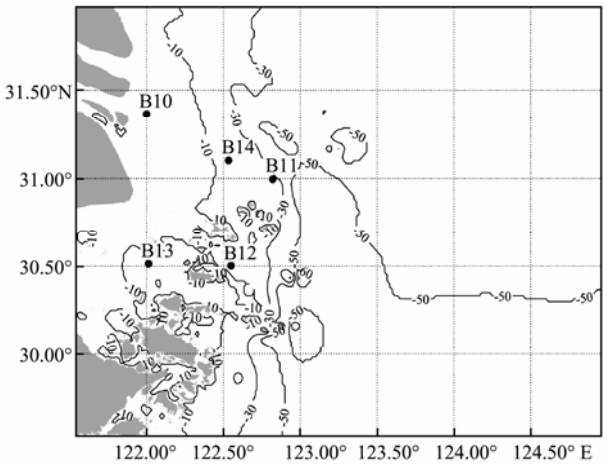

Fig.4 Locations of *in-situ* buoys around the Zhoushan Islands. The points and figures indicate the locations of the *in-situ* buoys. The contour lines indicate the water depths.

3.2 Validation of H-E Winds

As noted above, we simulated winds using the cyclone center, maximum wind radius r_{max}, central pressure p_c, and cyclone movement speed using the parametric Holland model with a 0.125° grid. We obtained four simulation results by setting different empirical scaling parameter B values of 0.4, 0.6, 0.8, and 1.0. We continuously selected the larger values between the ECMWF winds 10 m above the sea surface and the simulated winds of the Holland model. The composited wind fields are the H-E winds, which we validated against the collocated *in-situ* winds.

The five *in-situ* buoys recorded the winds and waves during tropical cyclone Fung-wong from September 19 to 30, 2014, and typhoon Chan-hom from July 8 to 16, 2015. In total, 282 wind-speed measurements from those buoys are available with winds up to 25 m s^{-1}.

Fig.5 shows comparisons of the simulation results from H-E winds and the buoy-measured wind-speed observations, which show a 2.35 m s^{-1} bias and 3.25 m s^{-1} root mean square error (*RMSE*) of the wind speed with constant B=0.4 in Fig.5a. A slightly larger 3.10 m s^{-1} bias and 4.71 m s^{-1} *RMSE* of wind speed is evident in Fig.5b for B = 0.6. Comparisons of the wind-speed observations and simulation results of H-E winds for B=0.8 and B=1.0 in Figs.5c and 5d, show a 3.76 m s^{-1} bias and a 6.07 m s^{-1} *RMSE* and a 4.34 m s^{-1} bias and 7.25 m s^{-1} *RMSE*, respectively. Interestingly, the major difference between the four data groups occurs at H-E wind speeds greater than 10 m s^{-1} and the comparisons also show that the wind-speed bias become greater as B increases. In other words, the H-E wind simulation results exhibit some increasing overestimations as B increases from 0.4 to 1.

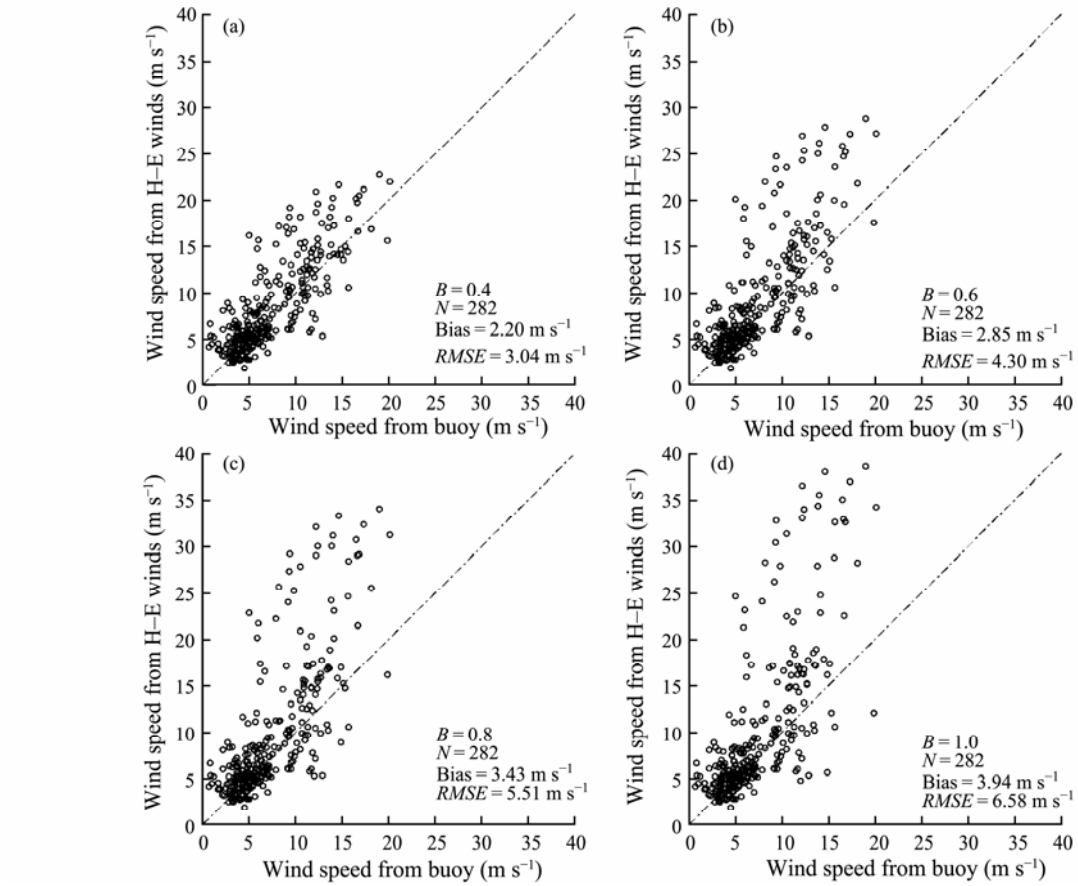

Fig.5 Comparisons of wind-speed observations from *in-situ* buoys and simulation results from H-E winds with different shape parameters B. (a) Shape parameter 0.4; (b) shape parameter 0.6; (c) shape parameter 0.8; (d) shape parameter 1.0.

Collectively, our statistical analyses of the simulation results from H-E winds for $B=0.4$ are better than the others. Therefore, in our study, we used H-E winds with $B=0.4$ as the input wind conditions of the WW3 model.

4 Evaluation of Source Terms

In this section, we briefly describe the WW3 model and investigate the performances of the seven input/dissipation terms. Then, we discuss the characteristics of the typhoon waves in typhoons Fung-wong and Chan-hom.

4.1 Brief Description of WW3 Model

Generally, the numeric WW3 model simulates waves by solving the following wave propagation balance equation:

$$\frac{\mathrm{D}}{\mathrm{D}t}\left(N\left(k,\theta;x,t\right)\right)=\frac{S\left(k,\theta;x,t\right)}{\sigma}, \tag{4}$$

$$N\left(k,\theta;x,t\right)=\frac{F\left(k,\theta;x,t\right)}{\sigma}, \tag{5}$$

in which the wavenumber-direction spectrum F is the basic spectrum of WW3, from which various spectra can be calculated; N is the wave action density spectrum; S shows the net sources and sinks from the wavenumber-direction spectrum; k is the wavenumber, θ is the wave direction, σ is the intrinsic frequency, and x and t represent the space and time coordinates, respectively. The net source and sink terms $S(k, \theta; x, t)$ contain the impacts of nonlinear wave propagation and partial wave reflections, because the total derivative of $N(k, \theta; x, t)$ normally considers linear propagation without scattering. Roughly speaking, the net source and sink term $S(k, \theta; x, t)$ consists of four parts, an atmosphere-wave interaction term S_{in}, a nonlinear wave-wave interaction term S_{nl}, a dissipation S_{ds}, and the empirical parameterizations of wave-bottom friction S_{bot}. Actually, the input term S_{in} and dissipation S_{ds} are associated, due to the fact that both mainly control the overall characteristics of the wave energy.

However, in our study, we considered two additional terms to simulate typhoon waves around the Zhoushan Islands. These are the depth-induced breaking S_{db}, which is important in numerical simulations in shallow water, and a linear input term S_{ln}, which provides more realistic initial wave growth. As mentioned above, the net source term $S(k, \theta; x, t)$ is defined as follows:

$$S=S_{\mathrm{ln}}+S_{\mathrm{in}}+S_{\mathrm{nl}}+S_{\mathrm{ds}}+S_{\mathrm{bot}}+S_{\mathrm{db}}. \tag{6}$$

These numeric simulations and parameterizations in the WW3 model are described in detail in the model's user manual (The WAVEWATCH-III Development Group, 2016), which we do not repeat here.

At present, the WW3 model provides several options for input/dissipation source terms for world-wide users, which can be employed depending on different sea states. Recently, the different input/dissipation sources terms of the previous WW3 model version (3.14), including ST1, ST2, ST2+STAB2, ST3, and ST3+STAB3, were validated against wave data from *in-situ* buoys and the Chinese HY-2 altimeter in the South China Sea (Wang *et al*., 2017a). Although the ST2+STAB2 source term package performs better than other source terms, its validation for application in typhoons has yet to be performed, especially in shallow waters. Among these source terms, seven terms, labeled ST1, ST2, ST2+STAB2, ST3, ST3+STAB3, ST4, and ST6 for convenience, work mainly for wave simulation. We describe these seven input/dissipation source terms in detail in the Appendix.

4.2 Validation of Simulated Waves

We simulated waves using the WW3 model for typhoon Fung-wong from September 1 to 30, 2014 and typhoon Chan-hom from July 1 to 31, 2015, for a total of 115 SWH observations during the period of typhoon Fung-wong and 96 during the period of typhoon Chan-horn. We used these data to validate the simulation results obtained by the WW3 model with the seven different input/dissipation source terms.

Fig.6 shows comparisons of the simulated SWHs and buoy measurements, in which (a), (b), (c), (d), (e), (f), and (g) represent ST1, ST2, ST2+STAB2, ST3, ST3+STAB3, ST4, and ST6, respectively. Tables 1 and 2 show the statistical analyses, including the biases and RMSEs of the different source terms, respectively.

4.3 Discussion

With respect to the validation results, the ST2 source term is the best optional source term for simulating typhoon waves in shallow waters around the Zhoushan Islands. We analyzed the performances of the seven source terms as follows. ST1 is assumed to be unsuitable for simulating regional ocean waves, because this input/dissipation source term is based on WAM3, which was developed for whole-ocean simulation. ST2+STAB2 tunes the simulations with deep-ocean wave growth, which means that the accuracy of the simulated results would be reduced in coastal waters and would be affected by the island chains, *e.g.*, Zhoushan Islands has more than 1000 islets. Therefore, its application is limited with respect to simulating waves in shallow water. ST3 is sensitive to swell and swell growth will reduce the dissipation as the swell portion increases. As a result, it is not adaptable for simulating waves in complex bathymetric topographies, although STAB3 considers high wind conditions. Similarly, the sensitivity of ST4 is also reduced as it takes into account the reducing drag coefficient in high wind conditions. ST6 is physically estimated based on measurements from lake experiments, but its performance must be further studied.

Next, we compared and analyzed the simulated SWHs from the WW3 model using the ST2 source term and the observations from individual buoys. Fig.7 shows the statistical results for typhoons Fung-wong and Chan-hom, in which we can see that the maximum bias and the largest

RMSE occurs at the location of the B13 buoy for both typhoons. The SWHs tend to result in positive biases with respect to the buoy measurements. We note that the B13 buoy is located in the area between Hangzhou Bay and the Zhoushan Islands.

As the typhoon waves propagate from open sea to land, they must cross a series of islands. Wave refraction and diffraction are inevitable due to the changes in topography, which may reduce the energy of long waves by 10%–20% (Sun *et al*., 2006) and result in wave breaking (Tolman, 2003). In addition, the water depth changes significantly due to storm surge or reduction during the typhoon period (Wang *et al*., 2017b). These factors can all be possible reasons for the overestimation of simulated SWHs and their inconsistency with the conclusions drawn from research in the Caribbean Sea and Gulf of Mexico (Liu *et al*., 2017). We plan to add switches related to the influence of islands in the WW3 model to improve the simulation results.

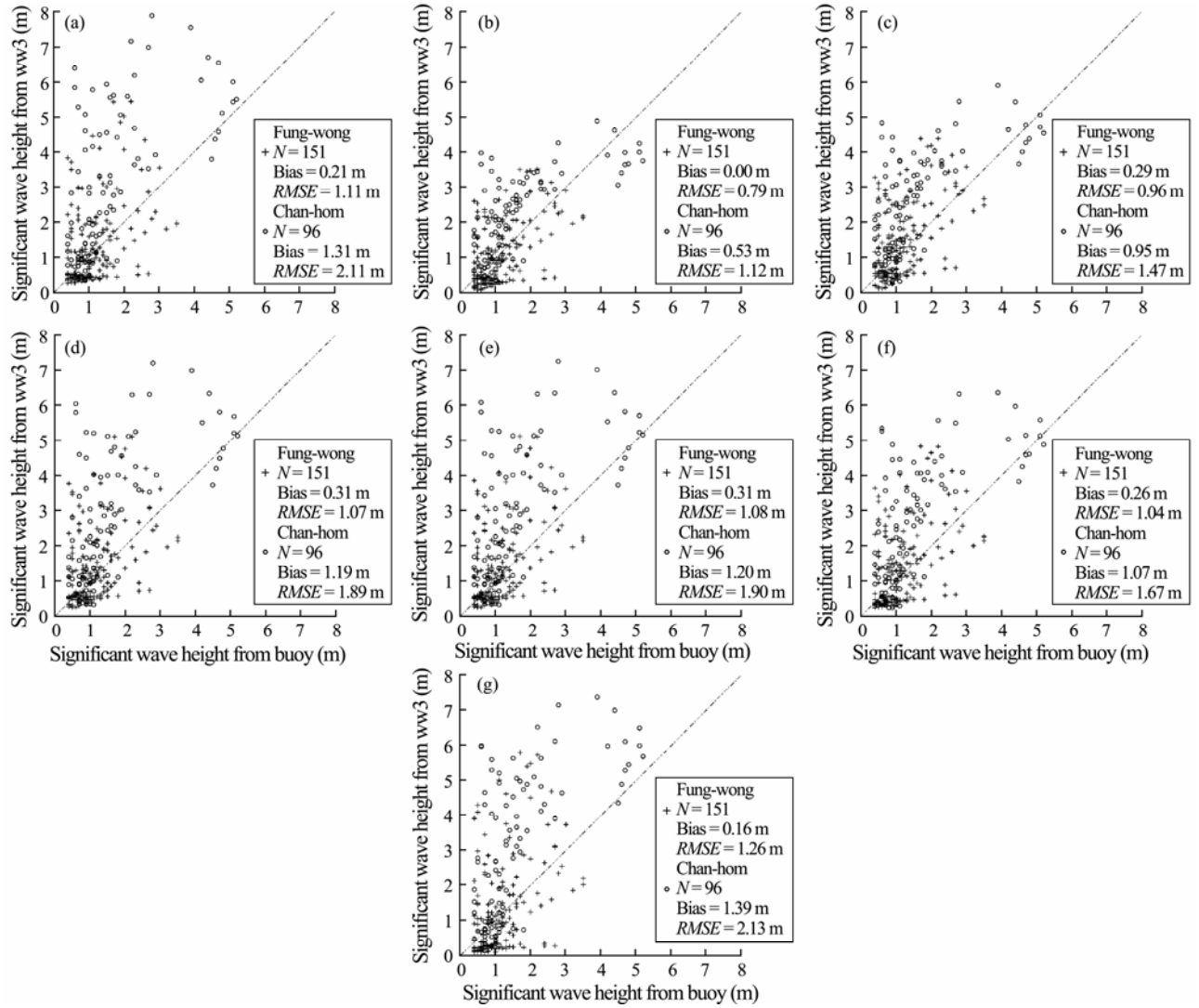

Fig.6 Comparisons of significant wave height observations from *in-situ* buoys and WW3 simulation results with different input and dissipation source terms, for tropical cyclone Fung-wong and typhoon Chan-hom. (a) ST1; (b) ST2; (c) ST2 +STAB2; (d) ST3; (e) ST3+STAB3; (f) ST4; (g) ST6.

Table 1 Comparison of WW3 simulations and buoy measurements during typhoon Fung-wong

Statistical indicator	ST1	ST2	ST2+STAB2	ST3	ST3+STAB3	ST4	ST6
Bias (m)	0.21	0.00	0.29	0.31	0.31	0.26	0.16
RMSE (m)	1.11	0.79	0.96	1.07	1.08	1.04	1.26

Table 2 Comparison of WW3 simulations and buoy measurements during typhoon Chan-hom

Statistical indicator	ST1	ST2	ST2+STAB2	ST3	ST3+STAB3	ST4	ST6
Bias (m)	1.31	0.53	0.95	1.19	1.20	1.07	1.39
RMSE (m)	2.11	1.12	1.47	1.89	1.90	1.67	2.13

Fig.8 shows the wave field during typhoon Fung-wong from September 21, 2014 at 18:00 UTC to September 23,

2014 at 00:00 UTC at 6-h intervals. In Fig.8a, we can see that the SWH above 4 m occupies most of area on September 21, 2014 at 18:00 UTC. As the typhoon moves, the maximum SWH is reduced to 3 m on September 23, 2014 at 00:00 UTC. Fig.9 shows the SWH fields in typhoon Chan-hom from July 9 to 14, 2015 at 06:00 UTC at 1-d intervals in the East China Sea. The SWH grew to 6 m when typhoon Chan-hom moved toward the East China Sea on July 9, 2015 at 06:00 UTC. As typhoon Chan-hom arrived at the Zhoushan Islands, the SWH exceeded 6 m on July 10, 2015 at 06:00 UTC. Afterwards, the SWH continued to reduce as typhoon Chan-hom moved to the northwest. The SWH had decrease to less than 1 m by July 14, 2015 at 06:00 UTC. It is not surprising that the SWH is smaller behind the island with respect to the wave propagation direction during the period of the two typhoons. However, the SWH significantly decreases as the waves propagate to shallow water around the Zhoushan Islands, *e.g.*, the maximum reduction is 3 m for typhoon Chan-hom.

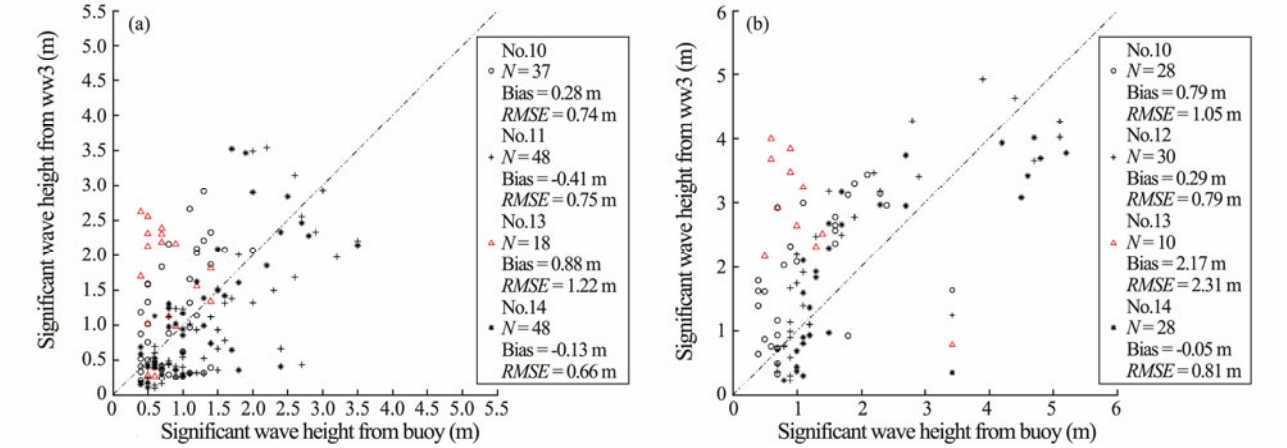

Fig.7 Comparisons of significant wave heights from WW3 and each buoy. (a) Comparisons of WW3 simulations and observations from each buoy during typhoon Fung-wong. (b) Comparisons of WW3 simulations and observations from each buoy during typhoon Chan-hom.

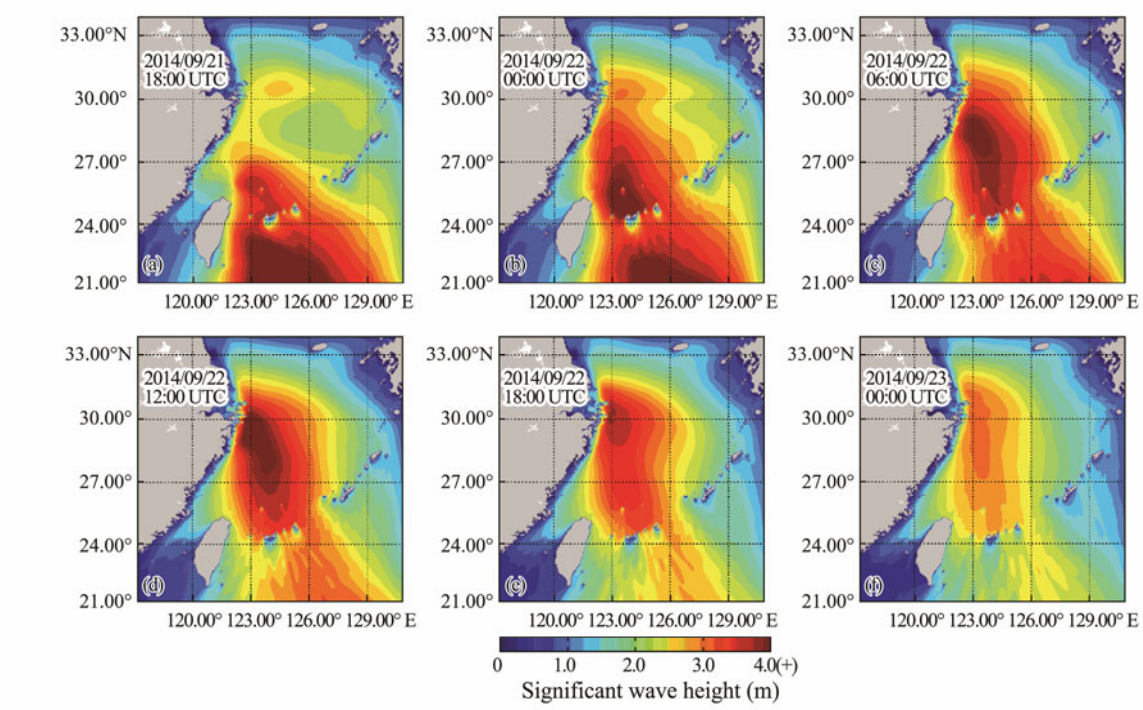

Fig.8 Wave fields during typhoon Fung-wong from September 21, 2014 at 18:00 UTC to September 23, 2014 at 00:00 UTC at 6-h intervals in the East China Sea. The colors indicate significant wave heights.

5 Summary and Conclusion

In this study, we systemically investigated the performance of the WW3 model (latest version 5.16) for typhoons Fung-wong and Chan-hom around the Zhoushan Islands, where the water is shallow, with depths less than 100 m. We used H-E winds as the model force, which is a compo-

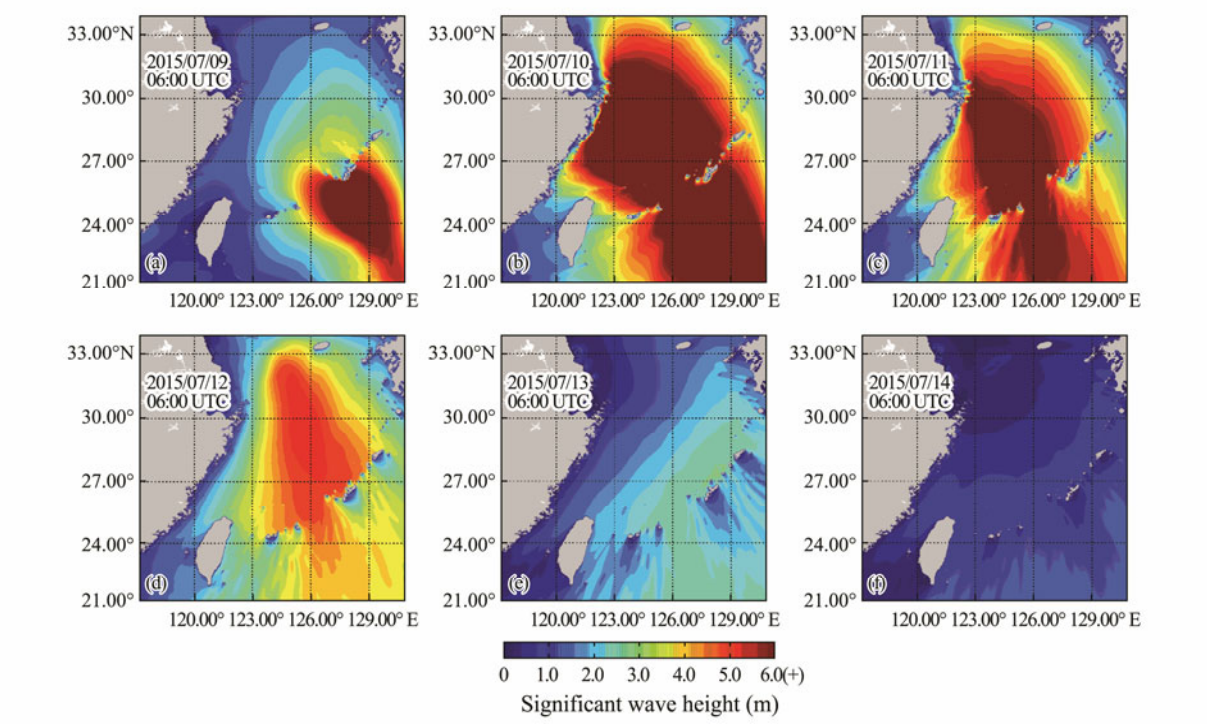

Fig.9 Wave fields during typhoon Chan-hom from July 9, 2015 to July 14, 2015 at 06:00 UTC at 1-d intervals in the East China Sea. The colors indicate significant wave heights.

sited of the simulation results from the parametric Holland model and ECMWF reanalysis wind data with a 0.125° grid. First, to obtain reasonable results, we had to determine how best to train the Holland winds, considering four scaling parameter B ranging from 0.4 to 1 at 0.2 intervals. We validated the H-E winds against wind-speed observations from five *in-situ* buoys during the typhoons Fung-wong and Chan-hom, and found that H-E winds for B= 0.4 performed better than the others, showing a 2.20 m s^{-1} wind-speed bias and a 3.04 m s^{-1} *RMSE* for wind-speed.

Then, to simulate the waves during the periods of the two typhoons, we applied seven kinds of input/dissipation source terms in the WW3 model, including ST1, ST2, ST2+STAB2, ST3, ST3+STAB3, ST4, and ST6. Our comparison of the waves observed by the five in-situ buoys in the typhoons show the ST2 input/dissipation source term to be the best option, with an RMSE for the SWH of 0.79 m and zero bias for typhoon Fung-wong and an *RMSE* for the SWH of 1.12 m and a 0.53-m bias for typhoon Chan-hom. Interestingly, the simulated SWHs at the B13 buoy located between Hangzhou Bay and the islands chain are overestimated compared to the buoy-measured SWHs. We think this is probably caused by the change in characteristics as the typhoon waves propagate across the islands.

We conclude that ST2 has a better capability for simulating typhoon waves around the Zhoushan Islands than the other input/dissipation sources terms. In the near future, we plan to add influence factors in simulations of typhoon waves using the WW3 model, *e.g.*, wave reflections due to islands, wave refraction due to changes in topography, and wave breaking. We also expect that the ST2 source term, together with the wave reflections and sub-grid, can be further improved with respect to wave simulations in typhoons around the Zhoushan Islands.

Appendix

WW3 provides seven input/dissipation terms in its latest version 5.16 for world-wide users, including ST1, ST2, ST2+STAB2, ST3, ST3+STAB3, ST4, and ST6 in SWITCH of WW3.

Switch ST1 represents the input and dissipation source terms of WAM3, which is based on the studies reported in Snyder *et al*. (1981) and Komen *et al*. (1984). The input and dissipation source terms are described as follows:

$$S_{\text{in}}(k,\theta)=C_{\text{in}}\frac{\rho_a}{\rho_w}\max\left[0,\left(\frac{28u_*}{c}\cos(\theta-\theta_w)-1\right)\right]\cdot\sigma N(k,\theta), \tag{A1}$$

$$u_*=u_{10}\sqrt{(0.8+0.065u_{10})\times10^{-3}}, \tag{A2}$$

$$S_{\text{ds}}(k,\theta)=C_{\text{ds}}\hat{\sigma}\frac{k}{\hat{k}}\left(\frac{\hat{\alpha}}{\hat{\alpha}_{PM}}\right)N(k,\theta), \tag{A3}$$

$$c=\frac{\sigma}{k}, \tag{A4}$$

where N is the wave action density spectrum; k is the wavenumber; θ is the wave direction; σ is the intrinsic frequency; C_{in} is a non-dimensional constant taken as 0.25; ρ_a is the density of air (=1.29 kg m^{-3}); ρ_w is the den-

sity of water (=1.025 kg m^{-3}); u_* is the wind friction velocity (Charmock, 1955; Wu, 1982); u_{10} is the wind speed 10 m above the sea surface; θ_w is the mean wind direction; $C_{ds}=2.36\times10^{-5}$, and the Pierson and Moskowitz (P–M) spectrum parameter $\alpha_{PM}=3.02\times10^{-3}$ (Pierson and Moskowitz, 1964).

Switch ST2 is an input/dissipation source term established by Tolman and Chalikov (1996, herein called TC96), which is described as follows:

$$S_{\text{in}}(k,\theta)=\sigma\beta N(k,\theta), \tag{A5}$$

$$S_{\text{ds}}(k,\theta)=AS_{\text{ds,l}}+(1-A)S_{\text{ds,h}}, \tag{A6}$$

where β is a non-dimensional wind-wave interaction parameter; and the dissipation source term $S_{\text{ds}}(k, \theta)$ combines the low-frequency dissipation $S_{\text{ds,l}}$ and high-frequency $S_{\text{ds,h}}$ by a linear parameter A, which is determined by wave frequency. The low-frequency dissipation $S_{\text{ds,l}}$ is the dominant dissipation similar to the wave energy dissipation caused by turbulence. It is defined as follows:

$$S_{\text{ds,l}}(k,\theta)=-2u_*hk^2\phi N(k,\theta), \tag{A7}$$

where h and ϕ represent a scaled mixture proportion and an empirical function of the growth state of the wave field, respectively (The WAVEWATCH-III Development Group, 2016), and u_* is the input wind speed. The high-frequency dissipation is expressed as follows:

$$S_{\text{ds,h}}(k,\theta)=a_0\left(\frac{u_*}{g}\right)^2 f^3\alpha_n^B N(k,\theta), \tag{A8}$$

$$B=a_1\left(\frac{fu_*}{g}\right)^{-a_2}, \tag{A9}$$

where α_n is a non-dimensional high-frequency Phillip energy level with a constant taken as 0.002, α_0=4.8, $\alpha_1=1.7\times10^{-4}$ and α_0=2.0.

Switch ST2+STAB2 shows a stable correction of the TC96 source terms. The TC96 source term is tuned for fetch-limited growth in the classical way, in that it reduces deep-ocean wave growth via global simulation test results. As such, Tolman (2002) gives an effective wind u_e instead of the wind speed u and a simple parameterization ST:

$$\frac{u_e}{u}=\left(\frac{c_0}{1+C_1+C_2}\right)^{-1/2}, \tag{A10}$$

$$C_1=c_1\tanh\left[\max\left(0,f_1\{ST-ST_0\}\right)\right], \tag{A11}$$

$$C_2=c_2\tanh\left[\max\left(0,f_1\{ST-ST_0\}\right)\right], \tag{A12}$$

$$ST=\frac{hg}{u_h^2}\frac{T_a-T_s}{T_0}, \tag{A13}$$

$$f_2=\frac{f_1c_1}{c_2}, \tag{A14}$$

where ST is a stability parameter; T_a, T_s and T_0 are the air, sea, and reference temperatures, respectively; c_0=1.4, c_1=−0.1, c_2=0.1, f_1=−150, and ST_0=−0.01. We note that the effective wind speed was derived 10 m above the sea surface.

Switch ST3 consists of the input source term of Janssen (2004) and the dissipation source term of Bidlot *et al*. (2005). The input source term is expressed as follows:

$$S_{\text{in}}(k,\theta)=\frac{\rho_a}{\rho_w}\frac{\beta_{\max}}{\kappa^2}e^z Z^4\left(\frac{u_*}{C}+z_\alpha\right)\cdot \cos^{P_{\text{in}}}(\theta-\theta_u)\sigma N(k,\theta)+S_{\text{out}}(k,\theta), \tag{A15}$$

where Z, as defined in the WW3 manual, is a function of the roughness length; κ is a von Kármán' constant (=0.4); a non-dimensional constant $\beta_{\max}$=1.2, P_{in}=2, z_α=0.011 and C is a constant. $S_{\text{out}}(k, \theta)$ is the linear decrease in swell:

$$S_{\text{out}}(k,\theta)=2s_1\kappa\left(\frac{\rho_a}{\rho_w}\right)^2\left[\cos(\theta-\theta_u)-\frac{\kappa C}{u_*\log(kz_0)}\right], \tag{A16}$$

where z_0 represents the roughness parameter and s_1 is generally set to 0.

The dissipation source term was developed by Bidlot *et al*. (2005) and its later modification is known as 'BJA' for Bidlot, Janssen, and Abdallah. The form of the general dissipation source term is as follows:

$$S_{\text{ds}}(k,\theta)^{\text{WAM}}=C_{\text{ds}}\bar{\alpha}^2\bar{\sigma}\left[\delta_1\frac{k}{\bar{k}}+\delta_2\left(\frac{k}{\bar{k}}\right)^2\right]N(k,\theta), \tag{A17}$$

$$\bar{k}=\left[\frac{\int k^pN(k,\theta)\mathrm{d}\theta}{\int N(k,\theta)\mathrm{d}\theta}\right]^{1/p}, \tag{A18}$$

$$\bar{\sigma}=\left[\frac{\int \sigma^pN(k,\theta)\mathrm{d}\theta}{\int N(k,\theta)\mathrm{d}\theta}\right]^{1/p}, \tag{A19}$$

$$\bar{\alpha}=E\bar{k}^2, \tag{A20}$$

where C_{ds}=−2.1 is a non-dimensional constant; δ_1=0.4, δ_2=0.6, p=0.5; $\bar{\sigma}$ and $\bar{\alpha}$ are the mean frequency and mean steepness, respectively, and E is the wave energy.

Switch ST3+STAB3 is a parameterization proposed by Abdalla and Bidlot (2002), which is included in the present parameterization to stabilize ST3 in unstable atmospheric conditions.

Switch ST4 is an input/dissipation source term proposed by Ardhuin *et al*. (2010). The form of this input source term is similar to Eq. (A15), except that the wind speed u_* is replaced by u'_*, which is defined as follows:

$$u'_* = \left|u_*^2(\cos\theta_u, \sin\theta_u) - |s_u|\right| \int_0^k \int_0^{2\pi} \frac{S_{\text{in}}(k',\theta)}{C} (\cos\theta, \sin\theta) \mathrm{d}k' \mathrm{d}\theta , \quad \text{(A21)}$$

where the stresses on high wind conditions are tuned by $|s_u| \sim 1$, and the dissipation source term is expressed as follows:

$$S_{\text{ds}}(k,\theta) = \sigma \frac{C_{\text{ds}}^{\text{sat}}}{B_r^2} \left[\begin{array}{c} \delta_d \max\{B(k) - B_r, 0\}^2 + \\ (1-\delta_d) \max\{B'(k,\theta) - B_r, 0\}^2 \end{array} \right] N(k,\theta) + S_{\text{bk,cu}}(k,\theta) + S_{\text{turb}}(k,\theta) , \quad \text{(A22)}$$

$$B(k) = \max\left\{B'(k,\theta), \theta \in [0, 2\pi]\right\} , \quad \text{(A23)}$$

where $B_r = 0.00085$, $\delta_d = 0.3$, and $C_{\text{ds}}^{\text{sat}} = 0$. Details regarding the saturation-based term $S_{\text{turb}}(k, \theta)$, cumulative breaking term $S_{\text{bk,cu}}(k, \theta)$ and a function B'(k, θ) are shown in manual 5.16 of the WW3 (The WAVEWATCH-III Development Group, 2016).

Switch ST6 is an input/dissipation source term based on measurements taken on lakes and in laboratory experiments. This term includes wind input and constraints, negative input, white capping dissipation, and swell dissipation (Zieger *et al*., 2015).

Acknowledgements

Source code for the WW3 model was kindly provided at no cost by National Centers for Environmental Prediction of National Oceanic and Atmospheric Administration (NOAA). We greatly appreciate the Institute of Oceanology, Chinese Academy of Sciences for providing wind and wave observations from *in-situ* buoys. The European Center for Medium-Range Weather Forecasts (ECMWF) wind data were openly accessed from http://www.ecmwf.int. The General Bathymetry Chart of the Oceans (GEBCO) data were downloaded *via*: ftp.edcftp.cr.usgs.gov. Typhoon parameters were provided by the Regional Specialized Meteorological Center (RSMC) Tokyo-Typhoon Center of Japan Meteorological Agency (JMA) *via* http://www.jma.go.jp. This research is partly supported by the National Key Research and Development Program of China under contract (Nos. 2017YFA0604901, 2016YFC 1401002 and 2016YFC1402000); the National Natural Science Foundation of China under contract (Nos. 41776 183, 41606024 and 41506033).

References

Abdalla, S., and Bidlot, J. R., 2002. Wind gustiness and air density effects and other key changes to wave model in CY25R1 ECMWF Research Department Technical Report Memorandum R60.9/SA/0273. European Center for Medium-Range Weather Forecasts, England.

Ardhuin, F., Rogers, E., Babanin, A. V., Filipot, J. F., Magne, R., Roland, A., Van Der Westhuysen, A., Queffeulou, P., Lefevre, J. M., Aouf, L., and Collard, F., 2010. Semiempirical dissipation source functions for ocean waves. Part I: Definition, calibration, and validation. *Journal of Physical Oceanography*, **40** (9): 1917-1941.

Bidlot, J. R., Abdalla, S., and Janssen, P., 2005. A revised formulation for ocean wave dissipation in CY25R1. ECMWF Research Department Technical Report Memorandum R60.9/JB/0516. European Center for Medium-Range Weather Forecasts England.

Bi, F., Song, J. B., Wu, K. J., and Xu, Y., 2015. Evaluation of the simulation capability of the Wavewatch Ⅲ model for Pacific Ocean wave. *Acta Oceanologica Sinica*, **34** (9): 43-57.

Charmock, H., 1955. Wind stress on a water surface. *The Quarterly Journal of the Royal Meteorological Society*, **81** (350): 639-640.

Guan, C. L., 2000. Review and prospect of wave theory and forecast research in China. *Journal of Ocean University of Qingdao*, **30** (4): 549-556 (in Chinese with English abstract).

Holland, G. J., 1980. An analytic model of the wind and pressure profiles in hurricanes. *Monthly Weather Review*, **108** (8): 1212-1218.

Janssen, P., 2004. *The Interaction of Ocean Waves and Wind*. Cambridge University Press, Cambridge, 169-268.

Kong, C. Y., Shi, J., Li, R. J., Yu, D. S., and Pan, X. S., 2013. Numerical simulation of typhoon waves around the waters in China's offshore. *Marine Environmental Science*, **32** (3): 419-423.

Komen, G. J., Hasswlmann, S., and Hasselmann, K., 1984. On the existence of a fully developed wind-sea spectrum. *Journal of Physical Oceanography*, **14** (8): 1271-1285.

Liu, Q. X., Babanin, A., Fan, Y., Zieger, S., Guan, C. L., and Moon, I. J., 2017. Numerical simulations of ocean surface waves under hurricane conditions: Assessment of existing model performance. *Ocean Modelling*, **118**: 73-93.

Pierson, W. J., and Moskowitz, L., 1964. A proposed spectral form for fully developed wind seas based on the similarity theoy of S. A. Kitaigorodskii. *Journal of Geophysical Researcher*, **69** (24): 5181-5190.

Qi, Y., Chu, P. C., Shi, P., Mao, Q., and Fan, C., 2003. Analysis of significant wave heights from wwatch and topex/poseidon altimetry. *Acta Oceanologica Sinica*, **25** (4): 1-9.

Snyder, R. L., Dobson, F. W., Elliott, J. A., and Long, R. B., 2006. Array measurements of atmospheric pressure fluctuations above surface gravity waves. *Journal of Fluid Mechanics*, **102**: 1-59.

Sun, J., Guan, C. L., and Liu, B., 2006. Ocean wave diffraction in near-shore regions observed by synthetic aperture radar. *Chinese Journal of Oceanology and Limnology*, **24** (1): 48-56.

Tolman, H. L., and Booij, N., 1998. Modeling wind waves using wave number direction spectra and a variable wavenumber grid. *Global Atmosphere and Ocean System*, **6** (4): 295-309.

Tolman, H. L., and Chalikov, D. V., 1996. Source terms in a third-generation wind wave model. *Journal of Physical Oceanography*, **26** (11): 2497-2518.

Tolman, H. L., 2002. Validation of WAVEWATCH III Version 1.15 for a Global Domain. *Technical Note 213*. National Oceanic and Atmospheric Administration. Camp Springs, US.

Tolman, H. L., 2003. Treatment of unresolved islands and ice in wind wave models. *Ocean Modelling*, **5** (3): 219-231.

The WAMDI Group, 1988. The WAM Model – A third generation ocean wave prediction model. *Journal of Physical Oceanography*, **18** (12): 1775-1810.

The WAVEWATCH-III Development Group, 2016. User manual and system documentation of WAVEWATCH III version 5.16. *Technical Note 329*. National Oceanic and Atmospheric Ad-

ministration. Camp Springs, US.

Wang, J., Zhang, J., Yang, J., Bao, W., Wu, G., and Ren, Q., 2017a. An evaluation of input/dissipation terms in wavewatch III using *in situ*, and satellite significant wave height data in the South China Sea. *Acta Oceanologica Sinica*, **36** (3): 20-25.

Wang, Z. F., Zhou, L. M., Li, Q. J., and Sun, X. J., 2017b. Storm surge along the Yellow River Delta under directional extreme wind conditions. *Journal of Coastal Research*, **80**: 86-91.

Wu, J., 1982. Wind-stress coefficients over sea surface from breeze to hurricane. *Journal of Geophysical Research Oceans*, **87** (C12): 9704-9706.

Xu, F. M., Perrie, W., Zhang, J. L., Song, Z. Y., and Bechara, T., 2005. Simulation of typhoon-driven waves in the Yangtze Estuary with multiple-nested wave models. *China Ocean Engineering*, **19** (4): 613-624.

Zec, J., and Jones, W. L., 2000. Scatterometer-retrieved hurricane wind direction ambiguity removal using spiral dealias. *Proceeding of IEEE International Geoscience and Remote Sensing Symposium*, Honolulu, USA, 24-28.

Zheng, K. W., Sun, J., Guan, C. L., and Shao, W. Z., 2016. Analysis of the global swell and wind sea energy distribution using WAVEWATCH III. *Advances in Meteorology*, **2016** (7): 1-9.

Zhou, L. M., Li, Z. B., Mou, L., and Wang, A. F., 2014. Numerical simulation of wave field in the South China Sea using WAVEWATCH III. *Chinese Journal of Oceanology and Limnology*, **32** (3): 656-664.

Zieger, S., Babanin, A. V., Rogers, W. E., and Young, I. R., 2015. Observation-based source terms in the third-generation wave model WAVEWATCH. *Ocean Modeling*, **96** (1): 2-25.

(Edited by Chen Wenwen)